Electrocatalysis Hot Paper

DOI: 10.1002/ange.201402315

Ultrathin WS_2 Nanoflakes as a High-Performance Electrocatalyst for the Hydrogen Evolution Reaction**

Liang Cheng, Wenjing Huang, Qiufang Gong, Changhai Liu, Zhuang Liu, Yanguang Li,* and Hongjie Dai*

Abstract: *Much has been done to search for highly efficient and inexpensive electrocatalysts for the hydrogen evolution reaction (HER), which is critical to a range of electrochemical and photoelectrochemical processes. A new, high-temperature solution-phase method for the synthesis of ultrathin WS_2 nanoflakes is now reported. The resulting product possesses monolayer thickness with dimensions in the nanometer range and abundant edges. These favorable structural features render the WS_2 nanoflakes highly active and durable catalysts for the HER in acids. The catalyst exhibits a small HER overpotential of approximately 100 mV and a Tafel slope of 48 mV/decade. These ultrathin WS_2 nanoflakes represent an attractive alternative to the precious platinum benchmark catalyst and rival MoS_2 materials that have recently been heavily scrutinized for the electrocatalytic HER.*

Hydrogen is frequently advocated as the alternative energy carrier of the future by virtue of its high energy density and zero environmental impact of the combustion product.[1,2] Its sustainable production from the splitting of water molecules driven by renewable solar energy has attracted tremendous attention because of its potential impact on the way of energy generation.[2–4] To achieve the best efficiency, this key process usually demands the assistance of high-performance hydrogen evolution reaction (HER) electrocatalysts.[4] Although precious platinum group metals, such as platinum and palladium, have traditionally been the most efficient catalysts for the HER, the search for active alternatives that are abundant on earth has been actively pursued, and some encouraging progress has been made.[4]

A large amount of current research is devoted to layered MoS_2 structures because of their appealing electrocatalytic properties for the HER.[5–12] It has been proposed and experimentally corroborated that the active sites are situated in sulfided Mo edges.[5,6] Through proper compositional and structural engineering, this compound is able to catalyze hydrogen generation at small overpotentials of approximately 100 mV with remarkable durability in acidic medium.[8] WS_2 has an analogous structure to MoS_2, and these compounds share a set of physical and chemical properties. WS_2 was also found to be HER active more than 20 years ago.[13,14] However, there have only been a few scattered studies focusing on WS_2 based HER electrocatalysts to date.[7,15–19] Their electrocatalytic performance is also far from satisfactory with typical overpotentials of over 150 mV. Very recently, lithium intercalation followed by forced hydration was found to exfoliate bulk WS_2 into metastable tetragonal monolayered sheets (1T-WS_2).[16] Individually, these sheets exhibited excellent HER activity,[16] whereas collectively they displayed a strong propensity towards restacking and an irreversible phase transition to hexagonal 2H-WS_2,[2,21] which led to a significant deterioration of the electrochemical performance.[18] It was suggested that decorating WS_2 monolayers with nanoparticles could help alleviate the restacking problem, but the improvement was very limited.[18] It stays elusive whether or not WS_2 can be on par with or even surpass the HER activity of MoS_2 for practical applications. Herein, we describe an effective high-temperature solution-phase method for the synthesis of WS_2 nanoflakes with monolayer thickness, dimensions in the nanometer range, and abundant edges. The product was shown to be a highly active and durable HER catalyst in acids, matching the activity of MoS_2.

The synthesis started with dissolving and heating a WCl_6 precursor in a mixed solvent of oleylamine (OM) and 1-octadecene under N_2 atmosphere (Figure 1). Elemental sulfur dissolved in OM was injected into the resulting solution at 300 °C (see the Experimental Section). OM has a high boiling point of over 360 °C, and elemental sulfur displays a considerable solubility in this medium.[22] Together, these properties make OM an ideal solvent for the high-temperature solution-phase synthesis of sulfide nanocrystals.[23,24] During the course of the reaction, the tungsten precursor solution first gradually turned blue (Supporting Information Figure S1), probably because of the reaction between WCl_6 and OM, which gives rise to a tungsten–oleylamine (W–OM) complex.[23] Upon

[*] Dr. L. Cheng,[+] W. J. Huang,[+] Q. F. Gong, C. H. Liu, Prof. Z. Liu, Prof. Y. G. Li
Institute of Functional Nano & Soft Materials (FUNSOM)
Collaborative Innovation Center of Suzhou Nano Science and Technology, Soochow University, Suzhou, Jiangsu 215123 (China)
E-mail: zliu@suda.edu.cn
yanguang@suda.edu.cn
Prof. H. J. Dai
Department of Chemistry, Stanford University
Stanford, California 94305 (USA)

[+] These authors contributed equally to this work.

[**] L.C. is supported through a post-doctoral research program of Jiangsu Province (1202044C) and a post-doctoral fellowship from the science foundation of China (2013M531400). Z.L. acknowledges supports from the National Natural Science Foundation of China (51302180, 51222203, 51002100, and 51132006), the National "973" Program of China (2011CB911002, 2012CB932601), the Priority Academic Program Development of Jiangsu Higher Education Institutions, and the National Natural Science Foundation of Jiangsu Province (BK20130005, BK20130305). Y.L. acknowledges startup supports from Soochow University and the Program for Jiangsu Specially-Appointed Professors.

Supporting information for this article is available on the WWW under http://dx.doi.org/10.1002/anie.201402315.

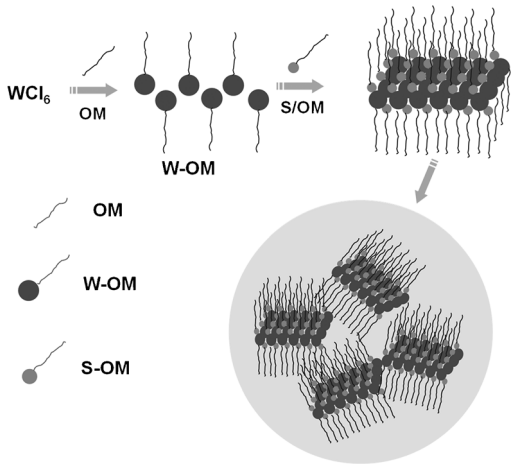

Figure 1. Synthesis of ultrathin WS_2 nanoflakes.

injection of the sulfur solution, the solution immediately turned black, suggesting rapid WS_2 formation (Figure S1). The as-made product was washed and finally annealed in argon atmosphere at 500 °C to remove any organic residues. We have explored a variety of synthetic parameters, such as solvents, precursor concentrations, reaction temperature, and time, and identified the current conditions as the most suitable for optimal product formation.

Scanning and transmission electron microscopies (SEM and TEM) were used to examine the microstructures of the final product. It appears to be particulate with a primary size in the range of 50–200 nm, as determined by SEM (Figure 2a). By high-resolution TEM, these primary particles were unraveled to be a collection of many loosely assembled WS_2 nanoflakes with mostly atomic thickness (Figure 2b,c). Even though we were unable to resolve individual nanoflakes because of their ultrathin thickness and poor contrast, the dark contrast lines in these images are believed to be the standing edges of WS_2 nanoflakes. The lack of clear orientational order over a large scale indicates that these ultrathin nanoflakes remain crystallographically independent within the primary particles. The lateral dimension of each WS_2 nanoflake was estimated to be about 5–20 nm. To probe the composition and spatial distribution of the constituent

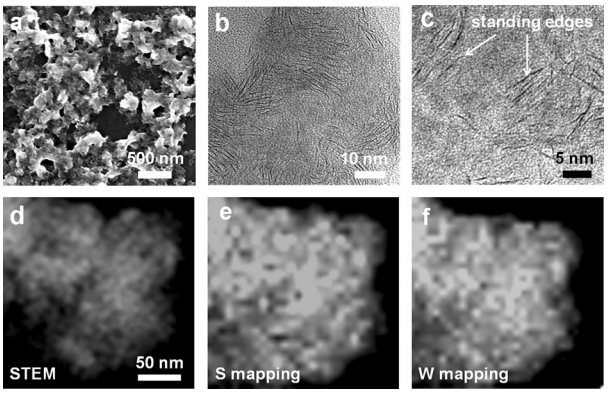

Figure 2. Microscopic characterization of WS_2 nanoflakes. a) SEM and b,c) high-resolution TEM images of WS_2 nanoflakes. Arrows in (c) mark the standing edges of monolayers. d) STEM image and e,f) EDS elemental maps of WS_2 nanoflakes.

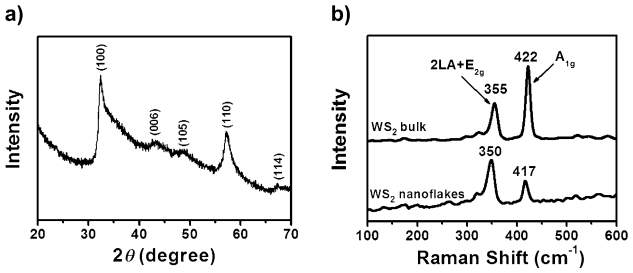

Figure 3. a) XRD pattern and b) Raman spectra of WS_2 nanoflakes.

elements, we carried out energy-dispersive X-ray spectroscopy (EDS) under scanning transmission electron microscopy (STEM). Tungsten and sulfur species were detected with a ratio close to 1:2 over a large area. Figure 2d–f shows the elemental mapping for tungsten and sulfur. Their distributions have a perfect spatial correspondence and are uniform throughout the primary particles. High-resolution tungsten and sulfur X-ray photoelectron spectra (XPS) of the WS_2 nanoflakes display peaks at binding energies characteristic of WS_2 (Figure S2).

The X-ray powder diffraction (XRD) pattern of the final product confirmed the identity of the hexagonal 2H-WS_2 phase with no discernible impurity (Figure 3a). The broadening of diffraction peaks reflects the nanoscale dimension of the final product. Most interestingly, both the (100) and (110) peaks exhibit an apparent asymmetry, reminiscent of the turbostratic stacking of layered compounds, which is commonly found in synthetic carbons and clays.[25,26] Turbostratically disordered layered compounds may be viewed as piles of randomly stacked sheets with no order between successive layers. The observed feature suggests that the WS_2 product does not crystallize well in all three dimensions, which is in accordance with the ultrathin thickness that was revealed through the above-mentioned high-resolution TEM analysis. We believe that the WS_2 nanoflakes are surface-passivated with solvent molecules. As a result, it is difficult for them to communicate and become in crystallographic order with one another. High-temperature annealing in the final step of the synthesis removes organic residues, but does not lead to restacking of the nanoflakes within the primary particles.

Further insight into the structure of the WS_2 nanoflakes was garnered from their Raman spectrum. Among many weaker peaks, it shows two pronounced peaks centered at 350 and 417 cm^{-1}, which are assignable to the longitudinal acoustic (2LA) and E_{2g} modes and the A_{1g} modes in 2H-WS_2, respectively (Figure 3b).[27] Importantly, the intensity of the $2LA + E_{2g}$ peak is approximately twice the intensity of the A_{1g} peak. It has been reported that under 514 nm laser excitation, the relative intensity of the former peak to the latter peak increases dramatically with decreasing WS_2 layer number, with a ratio greater than unity recorded only at the monolayer thickness.[27] Moreover, the frequency of the A_{1g} optical mode is also found to be sensitive to the number of WS_2 layers. It blue-shifts with an increase in layer number because of the increase in restoring force that is caused by van der Waals interactions among the layers.[27] Our ultrathin WS_2 nanoflakes exhibit an A_{1g} peak positioned at 417 cm^{-1}, which is in perfect agreement with the value reported for WS_2

monolayers.[27] All of these facts combined unambiguously corroborate the atomic thickness of individual WS_2 nanoflakes even though they further assemble to larger primary particles.

To assess their electrocatalytic performance in the HER, WS_2 nanoflake powders were thoroughly mixed with Ketjen superconducting carbon black and Nafion in a mixture of ethanol and H_2O and then drop-cast onto glassy carbon electrodes as the working electrode. Electrochemical measurements were carried out using the standard three-electrode setup with a saturated calomel electrode (SCE) and a graphite rod as the reference and counter electrodes, respectively (see the Experimental Section). For reference purposes, a commercial Pt benchmark (20 wt% Pt/C, Johnson Matthey), which is known to have negligible HER overpotentials, was included for comparisons side by side. Cyclic voltammetry (CV) curves show the normalized current density versus the potential for the WS_2 nanoflake catalyst along with the Pt benchmark and commercial WS_2 micropowders (Figure 4a). Electrocatalytic hydrogen evolution on the nanoflake catalyst begins at low cathodic potentials that correspond to an overpotential of approximately 100 mV, above which the HER current density increases rapidly. The HER overpotential observed with our nanoflake catalyst is superior to most values that have been reported for WS_2 based catalysts thus far, which have typical overpotentials of over 150 mV (Table S1).[7,15–19] It also compares favorably to some of the best MoS_2 based HER catalysts (MoS_2/rGO) that have been developed by us and other groups.[8] Tafel analysis of the HER polarization curves give rise to a slope of approximately 48 mV/decade for the WS_2 nanoflake catalyst (Figure 4b), which is far smaller than previously reported values.[7,15–19] It is close to the value of approximately 40 mV/decade observed with MoS_2, indicating a possible Volmer–Heyrovsky reaction pathway with electrochemical desorption of hydrogen as the rate-limiting step.[8] This is not surprising in light of the structural similarity between these two sulfide compounds. We also investigated the effect of the heat-treatment temperature on the electrocatalytic performance of the WS_2 nanoflakes (Figure S3). It seems that the as-made WS_2 product exhibits a much inferior performance, which is probably due to surface passivation with bulky organic molecules. Annealing at high temperatures ($\geq 500\,^{\circ}C$) decomposes the organic residues and exposes the active sites; however, too high an annealing temperature (such as 700 °C) may lead to aggregation of the product, thus giving rise to diminishing surface areas and hence lower HER activity.

Aside from a stringent requirement for high activity, another important criterion for electrocatalyst selection is good durability. To investigate the durability under electrocatalytic operation, the WS_2 nanoflake catalyst was continuously cycled for a total of more than 10000 cycles in H_2SO_4 (0.5 M). The electrocatalytic activity was periodically monitored by measuring the CV curves after every 1000 potential cycles and then plotting the change in cathodic current density at −0.42 V versus the SCE (Figure 4c). Experiments were performed both with a normal catalyst loading (0.35 mg cm^{-2}) and with an ultralow loading (0.07 mg cm^{-2}) to exclude an interference of the catalyst loading or film thickness with the results. Under both conditions, the cathodic current densities show a similar trend: They decrease initially but become stabilized after a couple of thousands of potential cycles. The CV curves of WS_2 nanoflakes before and after 10000 cycles are compared in Figure 4d. The activity loss appears to be small, corresponding to an increase in overpotential of < 10 mV. The remarkable durability indicates that the primary particulate structure of assembled WS_2 nanoflakes is highly stable and does not collapse or restack over the course of the cycling investigation.

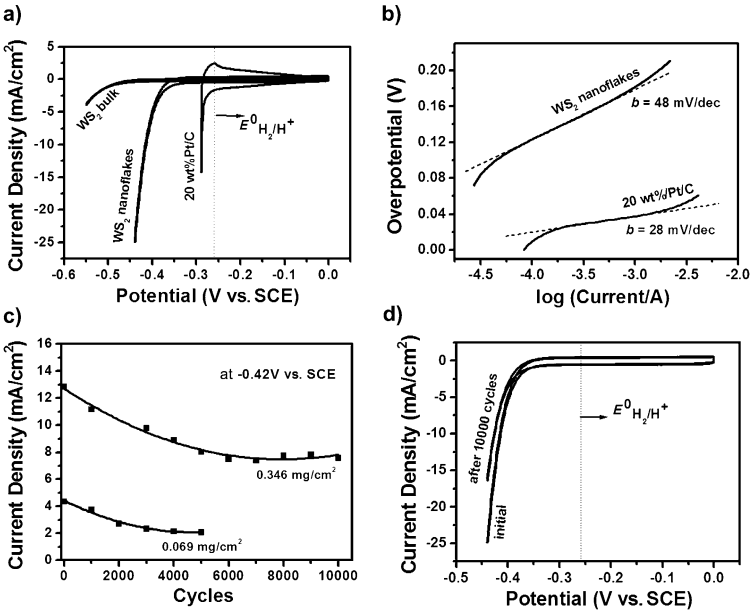

Figure 4. Electrochemical measurements for the WS_2 nanoflake catalyst in H_2SO_4 (0.5 M). a) CV curve of the WS_2 nanoflake catalyst along with those of the Pt benchmark catalyst and commercially available WS_2 micropowders. b) Corresponding Tafel plots. c) Change in the HER cathodic current density (at −0.42 V vs. SCE) with the number of potential cycles. d) CV curves of the WS_2 nanoflake catalyst before and after 10000 potential cycles. The theoretic value for the HER is indicated by dotted lines in (a) and (d).

We ascribe the excellent HER performance of our catalyst to its advantageous ultrathin nanoflake morphology with abundant accessible edges. HER active sites for MoS_2 are situated at sulfided Mo edges.[5,6] The structural analogy between MoS_2 and WS_2 prompted us to conjecture that the edge structure may also play a decisive role in HER electrocatalysis on WS_2. Unfortunately, layered WS_2 and MoS_2 crystals typically have a natural tendency to form closed fullerenes, nanotubes, or stacked multilayered geometries,[28–30] all of which have rather limited edge densities. Previously, the preparation of MoS_2 or WS_2 monolayers was only feasible through lithium intercalation and forced exfoliation of bulk materials.[11,16] These monolayers easily restack and risk losing their nanoscale features.[20,21] Here, we successfully prepared WS_2 nanoflakes with monolayer thickness and a size of 5–20 nm, as revealed by detailed structural characterization. Even though these nanoflakes further

assemble to form larger primary particles, they do not restack and still preserve their individual two-dimensional geometry with abundant accessible edges (Figure 1b,c), which are believed to contribute to the observed high HER activity.

In summary, we have developed a simple yet effective high-temperature solution-phase method for the synthesis of ultrathin WS_2 nanoflakes. This strategy leads to favorable monolayered nanosized products with abundant edges, which further assemble to form larger particulate structures. In acids, the WS_2 nanoflake catalyst exhibited efficient and durable activity for the hydrogen evolution reaction, with an impressively small overpotential of approximately 100 mV and a Tafel slope of 48 mV/decade. Given its excellent HER performance and low cost, this WS_2 nanoflake catalyst can compete with the extensively studied MoS_2 materials in every aspect of the performance and may find applications in a myriad of electrochemical or photoelectrochemical processes.

Experimental Section

Typical procedure for the synthesis of ultrathin WS_2 nanoflakes: WCl_6 (1 mmol) was added to a mixture of oleylamine (OM; 20 mL) and 1-octadecene (ODE; 10 mL) in a three-necked flask (50 mL) at room temperature. The solution was heated to 140 °C to remove water and oxygen under vigorous magnetic stirring in the presence of argon for protection for ca. 30 min. Afterwards, the temperature of the solution was rapidly raised to 300 °C and kept there for another 30 min in nitrogen atmosphere. A sulfur solution that was prepared by dissolving sulfur powder (2 mmol) in OM (5 mL) was then injected into the flask at 300 °C within 10 min. The reaction was kept at 300 °C for 1 h. After the reaction mixture had been cooled down to room temperature, WS_2 nanoflakes were precipitated by adding excess absolute ethanol (ca. 30 mL), collected by centrifugation, and washed repetitively with ethanol. To remove the organic residue, the as-made product was annealed in Ar at 500 °C for 2 h.

Characterizations: X-ray diffraction (XRD) was performed on a Shimadzu XRD-6000 X-ray diffractometer at a scanning rate of $0.05° s^{-1}$. Scanning electron microscopy (SEM) images were taken with a Zeiss scanning electron microscope. Transmission electron microscopy (TEM) and scanning transmission electron microscopy (STEM) were conducted on an FEI Tecnai F20 transmission electron microscope at an acceleration voltage of 200 kV. X-ray photoelectron spectra (XPS) were collected with an SSI S-Probe XPS Spectrometer. Raman spectra of powder samples were recorded on a LabRAM HR Raman microscope with a laser excitation wavelength of 514 nm.

Electrochemical measurements: WS_2 nanoflakes (1 mg), Ketjen black (0.5 mg), and a Nafion solution (5 wt %, 5 μL) were dispersed in a water/ethanol mixture (1:1, *v*/*v*; 0.2 mL) with the assistance of sonication (at least 30 min) to form a homogeneous ink. Then, 5 μL of the catalyst ink (containing 25 μg of catalyst) were loaded onto a glassy carbon electrode with a diameter of 3 mm (catalyst loading ca. $0.35 mg cm^{-2}$). Cyclic voltammetry (CV) was carried out in a standard three-electrode configuration at a scan rate of $10 mV s^{-1}$ with the glassy carbon electrode, a saturated calomel electrode, and a graphite rod as the working, reference, and counter electrodes, respectively. Tafel plots were collected at a scan rate of $5 mV s^{-1}$.

Received: February 12, 2014
Revised: March 24, 2014
Published online: May 18, 2014

Keywords: electrocatalysis · electrochemistry · hydrogen evolution reaction · monolayers · nanoflakes

[1] M. S. Dresselhaus, I. L. Thomas, *Nature* **2001**, *414*, 332 – 337.
[2] J. A. Turner, *Science* **2004**, *305*, 972 – 974.
[3] N. S. Lewis, D. G. Nocera, *Proc. Natl. Acad. Sci. USA* **2006**, *103*, 15729 – 15735.
[4] M. G. Walter, E. L. Warren, J. R. McKone, S. W. Boettcher, Q. Mi, E. A. Santori, N. S. Lewis, *Chem. Rev.* **2010**, *110*, 6446 – 6473.
[5] B. Hinnemann, P. G. Moses, J. Bonde, K. P. Jorgensen, J. H. Nielsen, S. Horch, I. Chorkendorff, J. K. Norskov, *J. Am. Chem. Soc.* **2005**, *127*, 5308 – 5309.
[6] T. F. Jaramillo, K. P. Jorgensen, J. Bonde, J. H. Nielsen, S. Horch, I. Chorkendorff, *Science* **2007**, *317*, 100 – 102.
[7] J. Bonde, P. G. Moses, T. F. Jaramillo, J. K. Norskov, I. Chorkendorff, *Faraday Discuss.* **2009**, *140*, 219 – 231.
[8] Y. Li, H. Wang, L. Xie, Y. Liang, G. Hong, H. Dai, *J. Am. Chem. Soc.* **2011**, *133*, 7296 – 7299.
[9] D. Merki, X. Hu, *Energy Environ. Sci.* **2011**, *4*, 3878 – 3888.
[10] J. Kibsgaard, Z. Chen, B. N. Reinecke, T. F. Jaramillo, *Nat. Mater.* **2012**, *11*, 963 – 969.
[11] M. A. Lukowski, A. S. Daniel, F. Meng, A. Forticaux, L. Li, S. Jin, *J. Am. Chem. Soc.* **2013**, *135*, 10274 – 10277.
[12] D. Kong, H. Wang, J. J. Cha, M. Pasta, K. J. Koski, J. Yao, Y. Cui, *Nano Lett.* **2013**, *13*, 1341 – 1347.
[13] A. Sobczynski, A. Yildiz, A. J. Bard, A. Campion, M. A. Fox, T. Mallouk, S. E. Webber, J. M. White, *J. Phys. Chem.* **1988**, *92*, 2311 – 2315.
[14] A. Sobczynski, A. J. Bard, A. Campion, M. A. Fox, T. E. Mallouk, S. E. Webber, J. M. White, *J. Phys. Chem.* **1989**, *93*, 401 – 403.
[15] Z. Wu, B. Fang, A. Bonakdarpour, A. Sun, D. P. Wilkinson, D. Wang, *Appl. Catal. B* **2012**, *125*, 59 – 66.
[16] D. Voiry, H. Yamaguchi, J. Li, R. Silva, D. C. B. Alves, T. Fujita, M. Chen, T. Asefa, V. B. Shenoy, G. Eda, M. Chhowalla, *Nat. Mater.* **2013**, *12*, 850 – 855.
[17] C. L. Choi, J. Feng, Y. Li, J. Wu, A. Zak, R. Tenne, H. Dai, *Nano Res.* **2013**, *6*, 921 – 928.
[18] J. Kim, S. Byun, A. J. Smith, J. Yu, J. Huang, *J. Phys. Chem. Lett.* **2013**, *4*, 1227 – 1232.
[19] J. Yang, D. Voiry, S. J. Ahn, D. Kang, A. Y. Kim, M. Chhowalla, H. S. Shin, *Angew. Chem.* **2013**, *125*, 13996 – 13999; *Angew. Chem. Int. Ed.* **2013**, *52*, 13751 – 13754.
[20] H.-L. Tsai, J. Heising, J. L. Schindler, C. R. Kannewurf, M. G. Kanatzidis, *Chem. Mater.* **1997**, *9*, 879 – 882.
[21] J. Heising, M. G. Kanatzidis, *J. Am. Chem. Soc.* **1999**, *121*, 11720 – 11732.
[22] J. W. Thomson, K. Nagashima, P. M. Macdonald, G. A. Ozin, *J. Am. Chem. Soc.* **2011**, *133*, 5036 – 5041.
[23] J. Joo, H. B. Na, T. Yu, J. H. Yu, Y. W. Kim, F. Wu, J. Z. Zhang, T. Hyeon, *J. Am. Chem. Soc.* **2003**, *125*, 11100 – 11105.
[24] Y. P. Du, Z. Y. Yin, J. X. Zhu, X. Huang, X. J. Wu, Z. Y. Zeng, Q. Y. Yan, H. Zhang, *Nat. Commun.* **2012**, *3*, 1177.
[25] T. N. Ramesh, R. S. Jayashree, P. V. Kamath, *Clays Clay Miner.* **2003**, *51*, 570 – 576.
[26] Z. Q. Li, C. J. Lu, Z. P. Xia, Y. Zhou, Z. Luo, *Carbon* **2007**, *45*, 1686 – 1695.
[27] A. Berkdemir, H. R. Gutierrez, A. R. Botello-Mendez, N. Perea-Lopez, A. L. Elias, C.-I. Chia, B. Wang, V. H. Crespi, F. Lopez-Urias, J.-C. Charlier, H. Terrones, M. Terrones, *Sci. Rep.* **2013**, *3*, 1755.
[28] R. Tenne, L. Margulis, M. Genut, G. Hodes, *Nature* **1992**, *360*, 444 – 446.
[29] L. Margulis, G. Salitra, R. Tenne, M. Talianker, *Nature* **1993**, *365*, 113 – 114.
[30] M. Remìkar, Z. Skraba, M. Regula, C. Ballif, R. Sanjines, F. Levy, *Adv. Mater.* **1998**, *10*, 246 – 249.

